Oceanologia (2016) 58, 176–186

Available online at www.sciencedirect.com

ScienceDirect

journal homepage: www.elsevier.com/locate/oceano

ORIGINAL RESEARCH ARTICLE

The impact of surface currents and sea level on the wave field evolution during St. Jude storm in the eastern Baltic Sea☆

Marili Viitak[a,*], **Ilja Maljutenko**[a], **Victor Alari**[b,1], **Ülo Suursaar**[c], **Sander Rikka**[a], **Priidik Lagemaa**[a,d]

[a] *Tallinn University of Technology, Marine Systems Institute, Tallinn, Estonia*
[b] *Helmholtz-Zentrum Geesthacht, Centre for Material and Coastal Research, Geesthacht, Germany*
[c] *University of Tartu, Estonian Marine Institute, Estonia*
[d] *Estonian Environment Agency, Estonian Weather Service, Estonia*

Received 5 October 2015; accepted 29 January 2016
Available online 16 February 2016

KEYWORDS
SWAN;
Wave–current–surge interaction;
Extreme storm;
Hindcast;
SAR

Summary A third generation numerical wave model SWAN (Simulating WAves Nearshore) was applied to study the spatio-temporal effect of surface currents and sea level height on significant wave height; and to describe the mechanisms responsible for wave–current interaction in the eastern Baltic Sea. Simulation results were validated by comparison with in situ wave measurements in deep and shallow water, carried out using the directional wave buoy and RDCP respectively, and with TerraSAR-X imagery. A hindcast period from 23 to 31 October 2013 included both a period of calm to moderate weather conditions and a severe North-European windstorm called St. Jude. The prevailing wind directions were southerly to westerly. Four simulations with SWAN were made: a control run with dynamical forcing by wind only; and simulations with additional inputs of surface currents and sea level, both separately and combined. A clear effect of surface currents and sea level on the wave field evolution was found. It manifested itself as an increase or decrease of significant wave height of up to 20%. The strength of the interaction was

☆ This study was financially supported by the Estonian Science Foundation Grant 9278, by institutional research funding IUT19-6 of the Estonian Ministry of Education and Research and by the Estonian Research Council grant PUT595.
* Corresponding author at: Tallinn University of Technology, Marine Systems Institute, Akadeemia tee 15a, 12618 Tallinn, Estonia. Tel.: +372 53803824.
E-mail address: viitak.marili@gmail.com (M. Viitak).
[1] Current address: Marine Systems Institute at Tallinn University of Technology, Estonia.
Peer review under the responsibility of Institute of Oceanology of the Polish Academy of Sciences.

Production and hosting by Elsevier

http://dx.doi.org/10.1016/j.oceano.2016.01.004

influenced by the propagation directions of waves and surface currents and the severity of weather conditions. An increase in the wave height was mostly seen in shallower waters and in areas where waves and surface currents were propagating in opposite directions. In deeper parts of the eastern Baltic Sea and in case of waves and surface currents propagating in the same direction a decrease occurred.

1. Introduction

In the event of a storm at sea, rough wave and severe surge conditions may lead to significant coastal and property damage or even to loss of life (e.g. Feser et al., 2015). Correct quantification of met-ocean parameters of a storm using numerical models and forecasting systems helps to reduce the storm related risks and mitigate consequences. Because in nature there is a feedback system between processes, detailed information about different interactions would provide us with a better understanding and improved predictability of hydrodynamic conditions at sea. For instance, an important feedback occurs between slowly-varying currents and highly varying waves. So far, the issue is little studied in the Baltic Sea.

The groundbreaking work of wave–current interaction was done by Longuet-Higgins and Stewart in a series of papers (1960, 1961, 1964). They described the interaction using radiation stress and demonstrated the energy transfer between waves and currents. Bretherton and Garrett (1968) introduced the idea of action conservation. Since then numerous papers have been published on the application of the theory including those by Wolf and Prandle (1999), Guedes Soares and de Pablo (2006) and Van der Westhuysen (2012). Alari (2013) studied the local storm surge effect on wave field in Pärnu Bay, Baltic Sea. He showed that sea level has a significant effect on wave field during extreme weather conditions. However, the effect of surface currents on wave field in the eastern Baltic Sea has had little attention.

The objectives of the present study were firstly, to assess the one-way interaction between waves, surface currents and sea level in almost tideless (up to 10 cm (Feistel et al., 2008)) coastal areas. We tried to find out the mechanisms by which surface currents and sea level rise influence the evolution of significant wave height under stormy conditions. This could help to improve modelling systems and see if it is worth further investigating the coupling of wave and hydrodynamic models in the Baltic Sea. Secondly, we studied the effect of spatial variability of surface currents and sea level on wave field. This would also indicate in which sea areas these interactions might be important during severe storms.

The paper is structured as follows: In Section 2 data and methods are presented including the description of measured and remotely sensed data and the description of numerical models and their set-ups. Section 3 presents the calculation results and discussion. The main conclusions and recommendations for further studies are summed up in Section 4.

2. Data and methods

2.1. Investigation area and measurements

The area of investigation is the eastern Baltic Sea, which is shown in Fig. 1. It includes two large gulfs – the Gulf of Finland and the Gulf of Riga. Water depth varies between 0 and 170 m. The Eastern section of the Baltic Sea, including the Gulf of Finland and Gulf of Riga, are extremely prone to storm surge (e.g. Wolski et al., 2014). The Gulf of Finland is connected with Baltic Proper with no barrier to the propagation of the waves, which allows, under certain meteorological conditions, long and high waves to enter the region (Leppäranta and Myrberg, 2009). According to Kahma and Petterson (1993) the mean significant wave height in spring is 0.5 m with peak period of 3.8 s and in winter 1.3 m with period of 5.3 s. Higher waves are produced in storm conditions (Soomere et al., 2008). In the Gulf of Riga wave propagation and growth are limited by shallow and narrow straits. Annual average wave height is between 0.25 and 0.5 m (Suursaar et al., 2012). According to Raudsepp et al. (2011) the peak period ranges between 2.3 and 8 s.

In Fig. 1 red and black squares show the stations where the measurements were taken for comparison with the simulations. Measurements in the Gulf of Finland (Fig. 1, station A) were conducted by the Finnish Meteorological Institute (FMI) at a site where water depth is 43 m. The device used was the

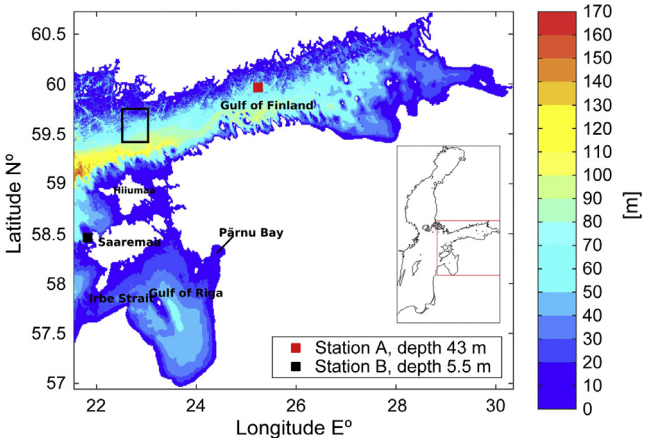

Figure 1 Eastern Baltic Sea bathymetry with grid resolution of 0.5 nautical miles. This area also represents the nested grid area. The black rectangle is the area of SAR measurements.

WAVERIDER MKIII directional wave buoy, which measures surface acceleration. Waves with period of 1.6 s and higher were registered. Measurements close to Saaremaa Island (Fig. 1, Station B) were conducted by the Estonian Marine Institute (Suursaar, 2013). The water depth at the measurement site was 5.5 m. The measurements were taken with a bottom mounted RDCP-600 (Recording Doppler Current Profiler), which measured the instantaneous dynamic pressure above its sensor. The pressure was further converted to surface elevation spectra with linear wave theory. Due to the attenuation of the pressure signal, there was a high-frequency cut-off and only waves with period of 2.6 s and bigger were measurable. As a result the realistic significant wave height can be higher than measured.

For remotely sensed data, a TerraSAR-X multi-look ground range detect (MGD) Stripmap product was used. The image was acquired with VV polarization and the pixel size was 1.25 m. Here the image acquired for the morning of 29 October 2013 (at 04:57 UTC) was used, which coincided with the storm maximum. The area of the image is shown on Fig. 1 as a black rectangle.

2.2. Numerical model

The SWAN model used in this study is a third-generation numerical wave model developed at the Delft University of Technology, in The Netherlands (Booij et al., 1999). Waves are described with the two-dimensional wave action density spectrum. The action density spectrum N is considered instead of the energy density spectrum E because in the presence of ambient currents, action density is conserved, but energy density is not. Action density is related to energy density through the relative frequency σ (Whitham, 1974):

$$N(\sigma,\theta) = \frac{E(\sigma,\theta)}{\sigma}. \tag{1}$$

Relative frequency is observed in a frame of reference moving with the current velocity, and θ is the wave propagation direction (the direction normal to the wave crest of each spectral component). SWAN solves the spectral action balance equation without any *a priori* restrictions on the spectrum for the evolution of wave growth (Booij et al., 1999). The action balance equation in Cartesian coordinates reads:

$$\frac{\partial N}{\partial t} + (c_g \rightarrow + u \rightarrow)\nabla_{x,y} N + \frac{\partial c_\sigma N}{\partial \sigma} + \frac{\partial c_\theta N}{\partial \theta} = \frac{S_{wind} + S_{nl3} + S_{nl4} + S_{wc} + S_{bot} + S_{db}}{\sigma}. \tag{2}$$

On the left-hand side of Eq. (2) the first term represents the local rate of change of action density in time; the second term denotes the propagation of wave energy in two dimensional geographical space, where $c_g \rightarrow$ is the group velocity and $\vec{u}$ is the ambient current. The third term represents the shifting of the relative frequency due to variations in depths and currents (with propagation velocity c_σ in σ space). The fourth term represents depth induced and current-induced refraction (with propagation velocity c_θ in θ space). On the right-hand side of the action balance equation is the source term that represents all physical processes which generate, redistribute or dissipate wave energy. These terms denote, respectively, wave growth by the wind S_{wind}, non-linear transfer of wave energy through three-wave S_{nl3} and four-wave interactions S_{nl4} and wave dissipation due to white-capping S_{wc}, bottom friction S_{bot} and depth-induced wave breaking S_{db} (The SWAN team, 2013a).

2.3. Accounting for currents and sea level in SWAN

The SWAN is not capable of calculating surface currents and sea levels. In order to take them into account they have to be presented as input. If there is no current or sea level input data, they are assumed to be zero (The SWAN team, 2013b).

2.3.1. Wind

Two mechanisms are used to describe the transfer of wind energy to waves – a resonance mechanism and a feed-back mechanism. For a more precise description see Phillips (1957) and Miles (1957). Wave growth is the sum of linear (A) and exponential (B) growth:

$$S_{wind}(\sigma,\theta) = A + BE(\sigma,\theta), \tag{3}$$

in which A and B depend on wave frequency and direction, and wind speed and direction. Linear wave growth contributes to the initial stages of wave growth. As the waves grow they start to affect the wind induced pressure field, which results in a larger energy transfer from the wind as the waves grow.

To account for the currents the apparent local wind speed and directions are used (The SWAN team, 2013a). In the presence of surface currents travelling opposite to the wave direction the transfer of wind energy to the waves is stronger and vice versa.

2.3.2. Kinematic effects

In Eq. (2) the kinematic effects are presented with left-side terms, except the time derivative term. As stated by Whitham (1974), wave energy propagation velocities in spatial and spectral space can be described by the kinematics of a wave train. In spatial space it reads:

$$\frac{d\vec{x}}{dt} = c_g \rightarrow + \vec{u} = \frac{1}{2}\left(1 + \frac{2|\vec{k}|d}{\sinh(2|\vec{k}|d)}\right)\frac{\sigma\vec{k}}{|\vec{k}|^2} + \vec{u}, \tag{4}$$

where k is wave number vector and d is the total water depth.

In spectral space:

$$c_\sigma = \frac{\partial\sigma}{\partial d}\left(\frac{\partial d}{\partial t} + \vec{u}\nabla_{x,y} d\right) - c_g\vec{k}\frac{\partial\vec{u}}{\partial s}, \tag{5}$$

$$c_\theta = \frac{-1}{k}\left(\frac{\partial\sigma}{\partial d}\frac{\partial d}{\partial m} + \vec{k}\frac{\partial\vec{u}}{\partial m}\right), \tag{6}$$

where s is the space coordinate in the wave propagation direction of θ and m is a coordinate perpendicular to s (The SWAN team, 2013a).

From kinematics in spatial space and spectral space (Eqs. (4)–(6)) it is observed that, when waves and currents are propagating in opposite directions, the second left-side term will be smaller in value in Eq. (2). This will result in an increase in the wave energy and therefore also in the wave

height. With waves and currents propagating in the same direction the effect is reversed.

As the sea level changes the total water depth influences the height of the waves. In nearshore regions, the group velocity decreases with decreasing water depth. To maintain a constant flux of energy transport an increase in the energy density occurs. This results in an increase of the wave height. With varying surface current and sea level refraction occurs (Eq. (6)).

2.3.3. Depth-induced wave breaking

Sea level will determine the maximum height of the waves beyond which the waves will start to break. Energy dissipation due to depth-induced wave breaking follows the analogy of breaking of a bore applied to random waves (Battjes and Janssen, 1978):

$$S_{db}(\sigma,\theta) = \frac{D_{tot}}{E_{tot}} E(\sigma,\theta), \tag{7}$$

where $D_{tot} = -\alpha_{BJ} Q_b \tilde{\sigma} H_{max}^2 (8\pi)^{-1}$ is the mean rate of energy dissipation per unit horizontal area due to wave breaking, $\alpha_{BJ} = 1$, $\tilde{\sigma}$ is the mean frequency, Q_b is the fraction of breaking waves and $H_{max}^2 = \gamma d$ is the maximum wave height that can exist at the given depth d where γ is the breaker parameter (set to 0.73). E_{tot} is the total wave energy integrated over all directions and frequencies (The SWAN team, 2013a).

During a surge the water depth deepens and the fraction of breaking waves reduces. This has the effect of moving the breaking zone towards the coast and increasing wave heights in coastal areas.

2.3.4. Whitecapping

Whitecapping is represented by the pulse-based model of Hasselmann (1974):

$$S_{wc}(\sigma,\theta) = -\Gamma \tilde{\sigma} \frac{k}{\tilde{k}} E(\sigma,\theta), \tag{8}$$

where $\tilde{k}$ is the mean wave number. The coefficient Γ depends on the overall wave steepness (The SWAN team, 2013a). In the presence of opposing currents waves experience enhanced whitecapping, because with opposing current wave number and wave steepness increases.

2.3.5. Bottom friction

The empirical model of JONSWAP (Hasselmann et al., 1973) is used to express bottom friction

$$S_{bot} = -C_b \frac{\sigma^2}{g^2 \sinh^2(kd)} E(\sigma,\theta), \tag{9}$$

where $C_b = 0.038\ m^2\ s^{-3}$ is the bottom friction coefficient (The SWAN team, 2013a).

As the surface currents affect the spectral wave energy, the bottom friction will also experience change. Bottom friction will increase with increasing wave energy e.g. in the case of an opposite current.

2.4. Model set-up and dynamical forcing

A nine-day period was chosen for the simulations, from 23.10.2013 to 31.10.2013. This includes calm to moderate weather conditions and a storm. In order to achieve realistic results in coastal areas, a nesting approach was used. The whole Baltic Sea region was simulated with a resolution of 1 nautical mile (nm). From there boundary conditions were obtained for the eastern Baltic Sea area, which had a resolution of 0.5 nm. The area of the 0.5 nm grid is shown in Fig. 1.

Table 1 Description of SWAN simulations.

r1 – simulation 1	(Reference simulation) wind
r2 – simulation 2	Wind and surface currents
r3 – simulation 3	Wind and sea level
r4 – simulation 4	Wind, surface currents and sea level

SWAN was forced with a 10 m wind field from the atmospheric model HIRLAM (Unden et al., 2002) interpolated on a model grid. HIRLAM wind fields had a spatial resolution of 11 km and a temporal resolution of 1 h. Additionally, input of surface currents and sea level were taken from the HIROMB model (Funkquist and Kleine, 2007; Lagemaa, 2012). Current values for the 1 nm grid were taken at a depth of 2 m. For the 0.5 nm grid the depth was 1.5 m. The SWAN computational grid and HIROMB horizontal grid were defined to be identical in order to avoid interpolation errors.

For bathymetry the Baltic Sea Bathymetry Database data was used (Baltic Sea Hydrographic Commission, 2013). Bathymetry was interpolated to the SWAN computational grid which was identical to HIROMB horizontal grid.

The integration time step for SWAN simulations was 10 min with directional bin width of 10°. Input fields of wind, currents and sea level to the wave model had a time step of 1 h. Output of SWAN was also requested once per hour.

Four simulations with SWAN were made using different dynamical forcings. Wind, surface currents and sea level were considered. In Table 1 there is a description of all the simulations. First a reference simulation with SWAN where there was only forcing by wind. On the second simulation, in addition to the wind, surface currents were included. With the third simulation, wind and sea level impact were taken into account. Finally, in the fourth simulation, all the dynamical forcings were present.

In this study it is assumed that the current and sea level are not affected by the wave field.

2.5. Wave parameters and statistics

The main focus of this study is to investigate the effects of hydrodynamics on significant wave height (Hs), which is defined as the mean height of the highest third of waves. In SWAN it is expressed as $Hs = 4\sqrt{\iint E(\omega,\theta)\, d\omega\, d\theta}$, where ω is the radian frequency.

To evaluate the performance of the model, four statistical parameters were calculated for simulations and measurements: the root mean square error (RMSE), the scatter index (SI), the mean deviation (BIAS) and the correlation coefficient:

$$RMSE = \sqrt{\frac{1}{N}\sum_{i=1}^{N}(a_i - b_i)^2}, \tag{10}$$

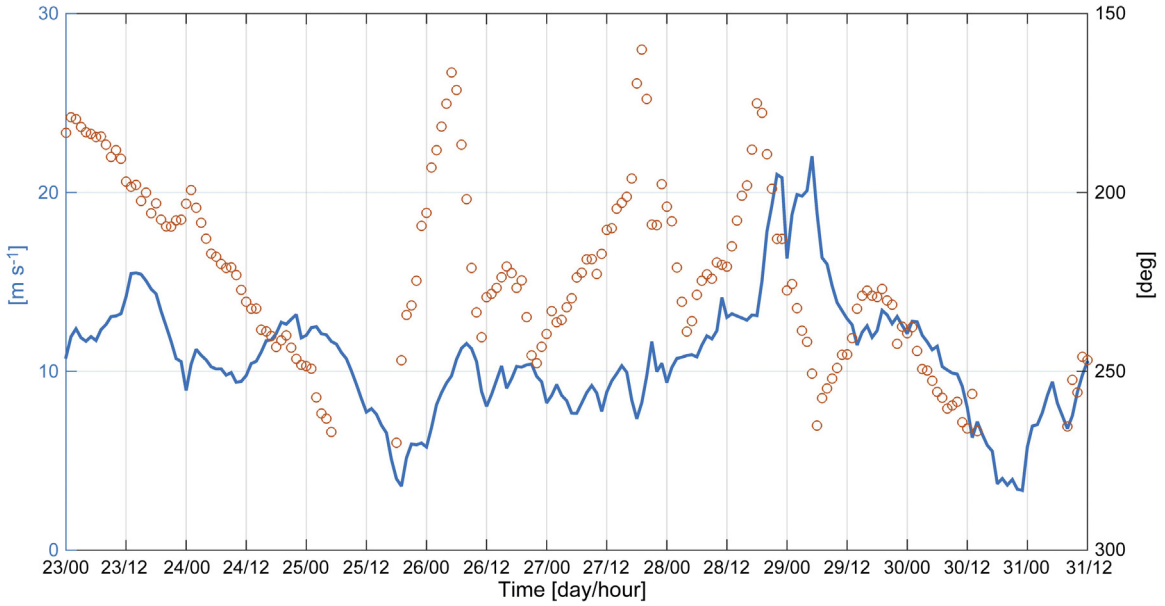

Figure 2 A time series of HIRLAM mean wind speed (blue line) and direction (red circles) near station B from modelling period 23.10.2013 to 31.10.2013. (For interpretation of the references to colour in this figure legend, the reader is referred to the web version of this article.)

$$\mathrm{SI} = \frac{\mathrm{RMSE}}{\frac{1}{N}\sum_{i=1}^{N} b_i} \times 100\%, \tag{11}$$

$$\mathrm{BIAS} = \frac{\sum_{i=1}^{N}(a_i - b_i)}{N}, \tag{12}$$

where a is the model data, b is the measurement and N is the number of elements.

In order to see the effects of different dynamical forcings, the significant wave height changes were studied by comparing the significant wave height of each model simulation ($n = 2, 3, 4$) with the reference simulation $n = 1$ at every time moment t:

$$\Delta\mathrm{Hs}^n(t) = \mathrm{Hs}^n(t) - \mathrm{Hs}^1(t). \tag{13}$$

To see the maximum range of possible change in significant wave height, the maximum difference over the time period of the storm day (whole day 29.10.2013) was calculated. The maximum difference $\Delta m\mathrm{Hs}^n$ for each grid point (lon,lat) was found as:

$$\Delta m\mathrm{Hs}^n = \Delta\mathrm{Hs}^n(t^n_{\max}), \tag{14}$$

where $t^n_{\max}$ (Eq. (15)) is the time when the difference of significant wave height (Eq. (13)) is maximum:

$$t^n_{\max} = argmax(|\Delta\mathrm{Hs}^n(t)|). \tag{15}$$

The maximum relative change was also calculated:

$$\Delta r\mathrm{Hs}^n = \frac{\Delta m\mathrm{Hs}^n}{\mathrm{Hs}^1} \times 100\%, \tag{16}$$

where

$$\mathrm{Hs}^1 = \mathrm{Hs}^1(t^n_{\max}), \tag{17}$$

and significant wave height of reference run r1 Hs^1 was found at time moment $t^n_{\max}$.

3. Results and discussion

3.1. Weather and sea state

A time series of HIRLAM 10 m mean wind speed and direction near the west coast of Saaremaa near measurement station B (see Fig. 1) is shown in Fig. 2.

From 23.10.2013 to 28.10.2013 mean wind speed ranges between 4 and 15 m s^{-1} which is considered to be calm to moderate weather. The storm, named St. Jude, lasted three days. It arrived in Estonia in the evening of 28.10.2013 and reached its highpoint in the early morning of the 29th. The weather started to calm down at the beginning of the next day.

At the peak of the storm, on 29.10.2013 at 04.00 mean wind speed, current velocity, sea level and significant wave height are shown in Fig. 3. During the storm the mean wind speed reaches 22 m s^{-1} (Fig. 3a). Wind was blowing from the sector S–SW, which is one of the most frequent wind directions in the Baltic Sea (Jaagus and Kull, 2011).

In Fig. 3b the simulated surface current velocities and propagation directions (every 10th vector is displayed) at the highpoint of the storm are displayed. Current speed reaches up to 195 cm s^{-1} in the Irbe strait. In the Gulf of Finland, in Pärnu bay and around Hiiumaa and Saaremaa the highest currents are up to 90 cm s^{-1}. The simulated surge reached up to 200 cm, compared to the model zero level (Fig. 3c). To the south east of Hiiumaa and Saaremaa, on the Finnish coast and in the Irbe strait the surge was up to 80 cm. In the deeper parts of the eastern Baltic it ranged from 80 to 100 cm. Simulated significant wave height (Fig. 3d) reached 6.5 m in the eastern Baltic Sea. Entering the Gulf of Finland and Gulf of Riga the wave height starts to decrease. Near the shore significant wave height is up to 2.5 m.

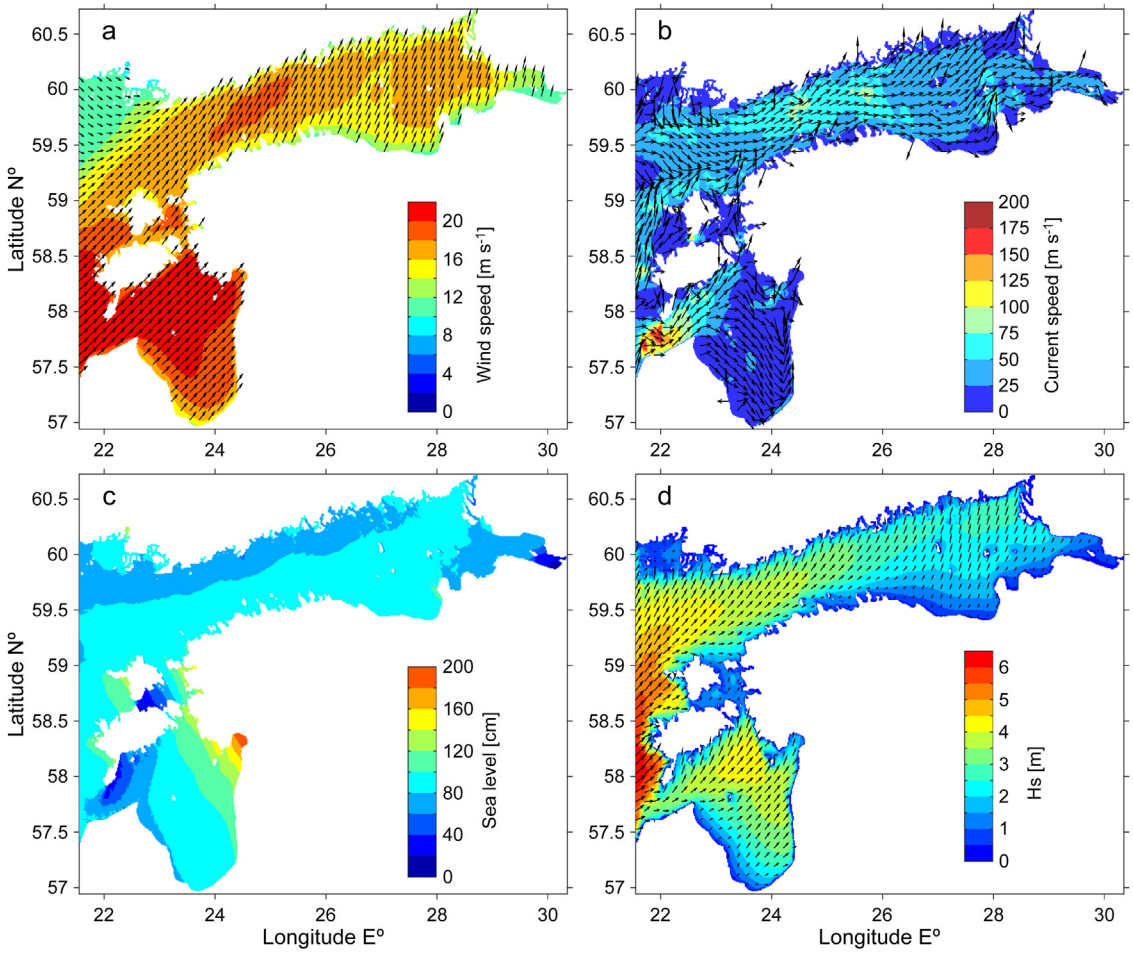

Figure 3 On 29.10.2013 at 04.00: (a) mean wind speed and direction (from HIRLAM model); (b) current velocity and direction (from HIROMB model); (c) the increase in the sea level (from HIROMB model); and (d) significant wave height (from SWAN model).

3.2. Comparison to measurements

Significant wave height is compared with measurements taken in deep water (depth 43 m) and close to the shore (measurement station A and B on Fig. 1, respectively). Wave direction is compared to SAR data. The model point chosen for comparison with station A is ca 200 m away with a water depth of 42.85 m.

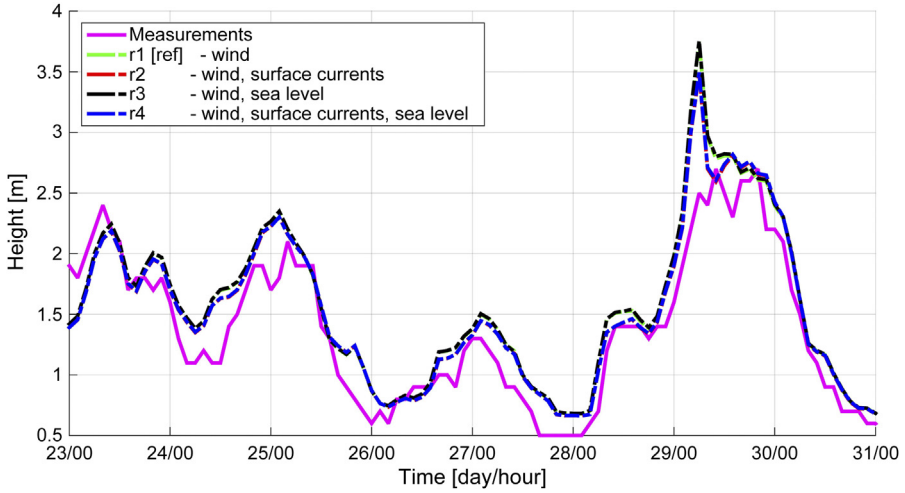

Figure 4 Comparison of measurements of significant wave height taken in Gulf of Finland in station A and SWAN simulations r1 to r4.

Table 2 RMSE, scatter index, BIAS and correlation coefficient are calculated from comparison of measurements in Gulf of Finland (measurement station A, Fig. 1) and model results. (a) In the time period from 23.10.2013 00.00 to 31.10.2013 23.00 – the whole modelling period. (b) Time period during the storm, 28.10.2013 00.00 to 30.10.2013 12.00.

	RMSE [cm]	Scatter index [%]	BIAS [cm]	Correlation coefficient
(a) 23.10.2013 00.00 to 31.10.2013 23.00				
Simulation 1	28	22	19	0.95
Simulation 2	25	19	15	0.95
Simulation 3	29	22	19	0.95
Simulation 4	25	19	16	0.95
(b) 28.10.2013 00.00 to 30.10.2013 12.00				
Simulation 1	36	21	26	0.95
Simulation 2	29	17	21	0.96
Simulation 3	37	22	27	0.95
Simulation 4	30	18	21	0.96

In Fig. 4, significant wave height from all four simulations (r1–r4) is compared. The time period for the validation in deep water covers the whole simulation period from 23.10.2013 to 31.10.2013. Simulated significant wave height follows the variability of the measurements well. In general the wave height is overestimated by the model in all runs. On 29.10.13 there is an unexpected overshoot in all the simulations. It is not caused by meteorological forcing time steps, as the wind is interpolated linearly over time for the model input. Simulations r2 and r4 show a slight improvement in the model results compared to r1 and r3.

Next the statistical parameters for significant wave height are calculated using Eqs. (10)–(12). Calculated over the period of 23.10.2013 00.00 to 31.10.2013 23.00 (Table 2a), the best results are produced with simulations r2 and r4, where surface currents are accounted for. RMSE for the reference simulation r1 is 28 cm, SI 22% and BIAS 19 cm. Taking into account currents (r2) RMSE decreases 3 cm, scatter index 3% and BIAS 4 cm. Considering only sea level in the simulations has a negative impact on the results. This may be due to the fact that the measurement point is situated in deep water. The study of Alari (2013) shows that sea level plays a more significant role in shallower waters. Correlation between measurements and the model is reasonably good, 0.95 for all the simulations.

Now looking separately at the statistics for the storm period 28.10.2013 00.00 to 30.10.2013 12.00 (Table 2b), it is apparent that accounting for surface currents improves the comparison significantly. As the RMSE of reference simulation r1 in storm conditions is 36 cm, it decreases when taking account of currents by 7 cm. The scatter index and BIAS also show improvement. Correlation goes from 0.95 (r1 and r3) to 0.96 (r2 and r4).

The *ad hoc* measurements at station B near Saaremaa Island lasted from 26.10.2013 to 31.10.2013. Measurements were taken at a location where there were large gradients in water depth. In the model bathymetry the closest point to the measurement station had a depth of 21.10 m. Therefore another point in shallower water, with depth of 7.83 m, was chosen as a comparison point. The latter point is ca 1 km away from station B.

In Fig. 5 it can be seen that, as with the deeper water, the model again overestimates measurements. Reference simulation r1 is closest to the measured results. Taking currents into account (r2), the significant wave height is overestimated even more. Considering sea level and also surface currents, both increase the wave height compared to simulations r1 and r2. In the case of current being accounted for, the increase of significant wave height can be explained by the changes in the group velocity of waves. With a decrease in the group velocity in the case of opposing current, in order to maintain energy flux, the wave energy density has to increase.

Model deviations from measurements increase when more dynamical forcings are added to the simulations (Table 3). This can be caused by several factors. In shallow water bottom effects occur, making the balance between wind, surface currents and sea level quite complicated. For example, unknown local bathymetrical features not resolved by the model may be the cause of increasing errors (Tuomi et al., 2014). While the water depth at station B was 5.5 m only,

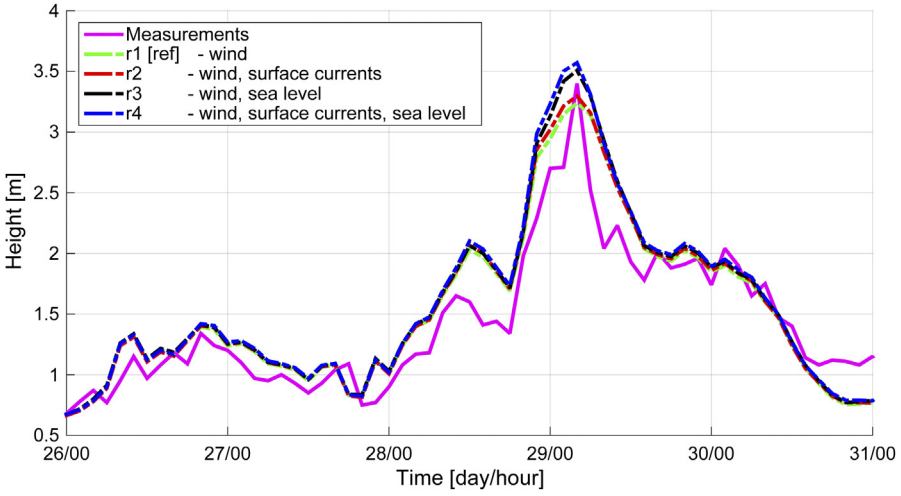

Figure 5 Comparison of measurements of significant wave height taken close to Saaremaa at station B and SWAN simulations r1 to r4.

Table 3 RMSE, scatter index, BIAS and correlation coefficient between measurements taken close to Saaremaa (measurement station B, Fig. 1) and model simulations.

Simulation	RMSE [cm]	Scatter index [%]	BIAS [cm]	Correlation coefficient
1	26	18	9	0.93
2	27	19	10	0.93
3	29	21	12	0.93
4	30	22	13	0.94

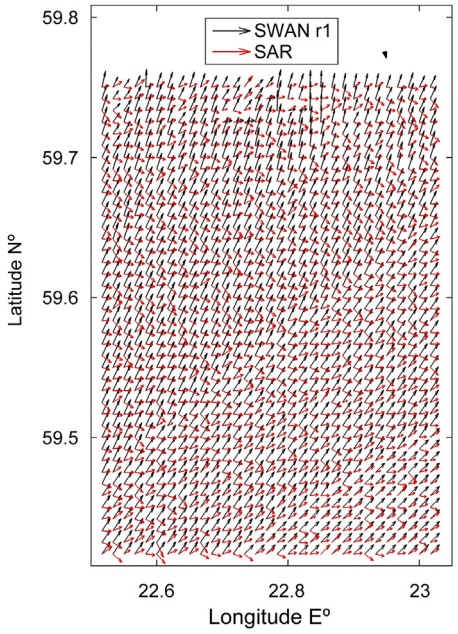

Figure 6 SWAN peak direction in simulation 1 (black arrows) are compared with SAR image (red arrows) on 29.10.2013 at 05.00. (For interpretation of the references to colour in this figure legend, the reader is referred to the web version of this article.)

Table 4 RMSE between SWAN and SAR peak directions.

	Simulation			
	1	2	3	4
RMSE [°]	47.10	49.01	47.08	48.94

water depth at the model point was 7.83 m. This calls for higher-resolution simulations, which are outside the scope of the present study.

Peak wave peak directions calculated with SWAN were compared to results from SAR images. The area of validation is shown in Fig. 1. In Fig. 6 SWAN reference simulation peak directions (red arrows) and directions provided by SAR (black arrows) are displayed. A moderate difference between the directions can be seen. In Table 4 RMSE of direction for all four simulations is presented. It varies between 47.08 and 49.01°. Simulation 3, where water level was included in the simulation, produces the best result, with RMSE of 47.08°.

3.3. Spatio-temporal impact of currents and sea-level

In order to quantify the impact of different dynamical forcings, the maximum difference of significant wave height $\Delta m\mathrm{Hs}^n$ and relative change $\Delta r\mathrm{Hs}^n$ were found with Eqs. (13)–(17). It was seen from the validations that current and sea-level effects are most noticeable during the St. Jude storm. For this reason the day of 29.10.2013 was chosen to evaluate the spatial variability of the wave field.

In Fig. 7 the probability density functions of spatial $\Delta m\mathrm{Hs}^n$ distribution are presented on a logarithmic scale. It shows the distribution of maximum difference of significant wave height. With simulation r2 (red line), where wind and surface currents were taken into account, there is a decrease in the wave height of up to 50 cm and an increase as big as 40 cm compared to r1. When taking account of wind and sea level (r3, black line) the difference ranges from −10 to 100 cm. With varying sea level the increase in the wave height is more evident. This should be the case, since with increased water

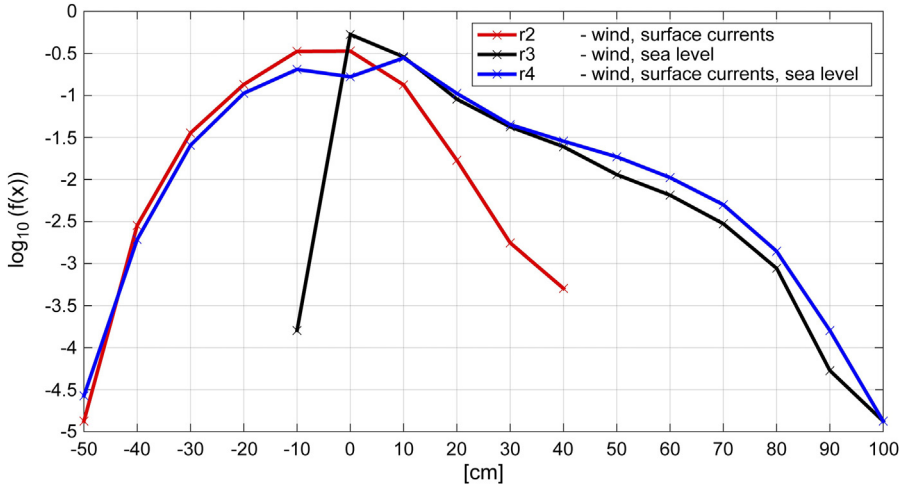

Figure 7 Significant wave height maximum differences $\Delta m\mathrm{Hs}^n$ logarithmical probability distribution for simulations r2, r3 and r4 on 29.10.2013.

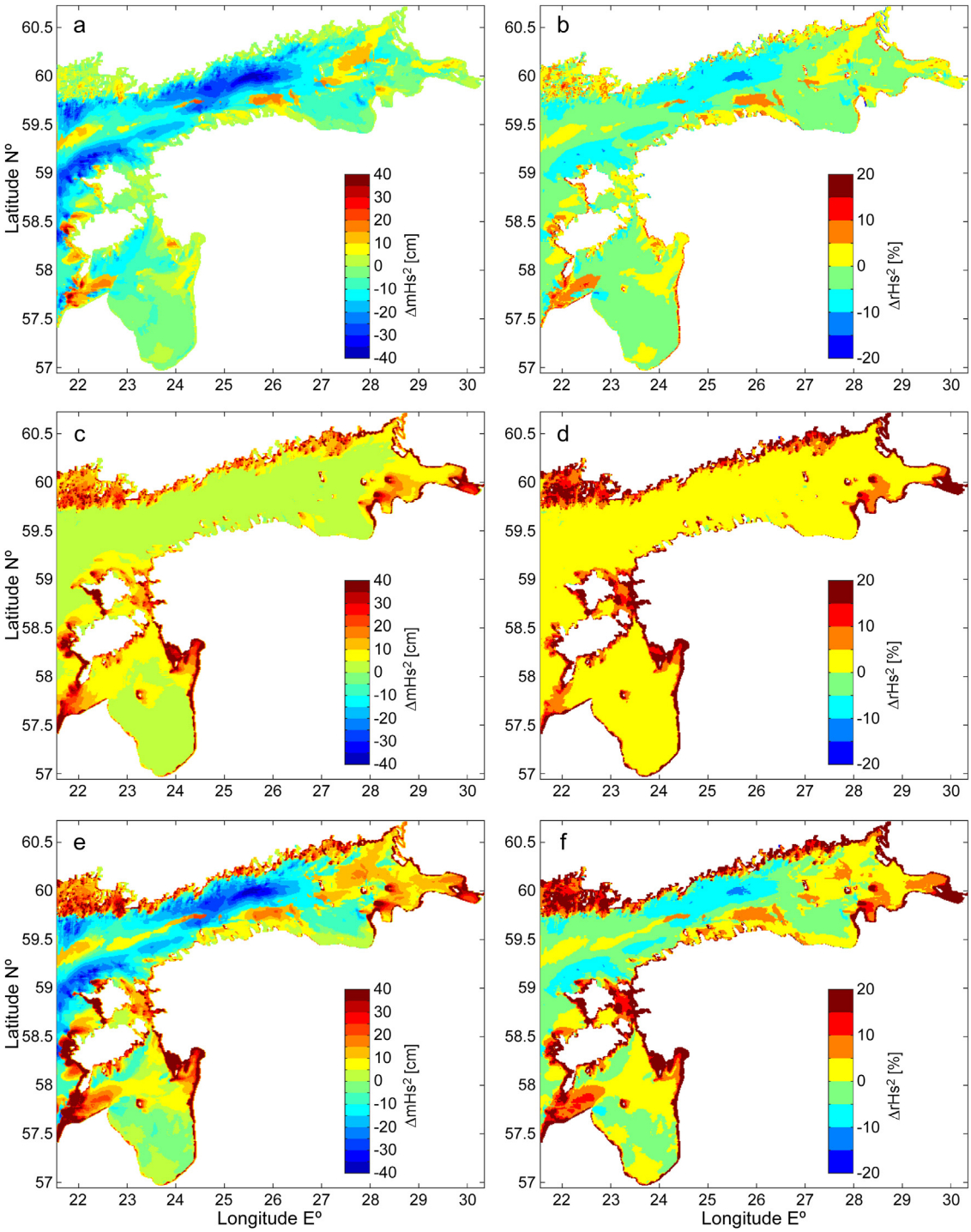

Figure 8 Time maximum absolute difference $\Delta m\mathrm{Hs}^n$ and relative difference $\Delta r\mathrm{Hs}^n$ in the significant wave height. (a and b) for r2; (c and d) for r3; (e and f) for r4. Values in a range −40 to 40 cm and −20 to 20% are shown in the figure.

level the dissipation is less. Accounting for all the dynamical forcings, the difference of $\Delta m\mathrm{Hs}^4$ ranges from −50 to 100 cm.

Next the spatial variability of maximum difference of significant wave height $\Delta m\mathrm{Hs}^n$ is shown in Fig. 8 on the left side and relative change $\Delta r\mathrm{Hs}^n$ on the right side. The colour bar ranges from −40 cm to 40 cm in the case of absolute differences and from −20% to 20% for the relative changes.

In Fig. 8a and b the maximum absolute difference and relative change in the significant wave height when taking account of surface currents (r2) is shown. Increase in the wave height is most evident near coasts and in narrow straits. In the southern part of the Gulf of Finland near the coast there is an increase of up to 10 cm (5%). In the north-east of the Gulf of Riga there is an increase of up to 20 cm (10—15%). Near the west coast of Hiiumaa wave height difference is about 10—20 cm (up to 20%). In Saaremaa and in the Irbe strait the difference can reach as much as 40 cm (up to 20%).

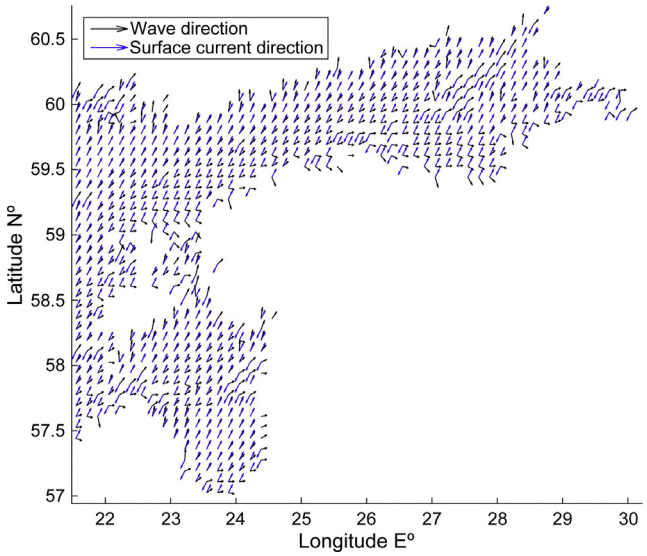

Figure 9 Propagation directions for waves in run r2 and surface currents on the time moments of maximum differences on 29.10.2013. Every 10th vector is displayed.

In Fig. 9 every 10th vector of wave and current propagation direction at time moment t_{max} (of simulation r2) are displayed. Wave directions are shown with black arrows and surface currents with blue arrows. As waves and surface currents approach opposite directions, currents have the effect of elevating wave height. For example in Fig. 9 in Pärnu bay, the Irbe strait and on the west coast of the islands Hiiumaa and Saaremaa the waves and surface currents are propagating in opposite directions (or the current direction is deflected right of the wave directions). This results in a greater wave height increase, seen also in Fig. 8a.

In the case of currents being accounted for, a decrease of the significant wave height occurs in deeper parts of the eastern Baltic Sea. In the Gulf of Riga and Gulf of Finland there is a decrease of up to 15 cm (5%). In the Gulf of Finland between 25–26°E and 58.8–60°N wave height decreases up to 40 cm (20%) (Fig. 8a and b). In Fig. 9 it is seen that in these areas waves and surface currents are propagating more or less in the same direction and this results in a decrease of significant wave height, which is also consistent with the theory.

It is likely that the maximum differences in significant wave height occur in a specific phase of the surface currents inertial oscillation. The magnitude of the increase and decrease of significant wave height is influenced by current velocity. For example in the Irbe strait the current velocity reaches up to 195 cm s^{-1} (Fig. 3b) and from Fig. 8a and b it is seen that in this area the significant wave height is one of the things most strongly affected by the surface currents.

In Fig. 8c and d the maximum difference and relative change of significant wave height when considering wind and sea level in the run (r3) is shown. In deeper parts of the eastern Baltic Sea, where the waves are not affected by the sea bed, there is an increase in the significant wave height of about 5 cm with relative increase of 5%. Near the coast, where the bottom effects come into play, a bigger increase in the wave height is noticeable. In coastal areas the maximum difference of significant wave height between reference run r1 and r3 is up to 40 cm (20%). Also in specific locations in the Gulf of Finland and in the Gulf of Riga there is a possible increase in wave height of 40%. It is seen that areas most significantly affected by sea-level are well exposed to the wind. This is also consistent with the work by Alari (2013).

In Fig. 8e and f it is shown the joint effect of surface currents and sea level on the wave field. On areas open to the wind the total impact of surface currents and sea level on wave height increases. For example in Pärnu bay when accounting for just currents the difference is up to 20 cm (10–15%), but the joint effect increases the wave height up to 40 cm (20%). The spatial variability patterns of surface current effects and sea level both remain. The decrease in the significant wave height remained more or less in the same areas where it was when there were just surface currents present.

4. Conclusions

Analysis of spatio-temporal patterns of wave–current–surge interaction in the eastern Baltic Sea and the corresponding mechanisms showed the impact of surface currents and sea level to the evolution of significant wave height. In deep (>20 m) water, surface currents improved the model-data comparison, especially in storm conditions. Variations in sea level had a negligible effect in deep waters, but in shallower water the effect of sea level was even larger than that of the surface currents. The extra increase in wave height was most noticeable in storm conditions and in wind exposed areas. During extreme storms, the joint effect of currents and sea level produced changes in the significant wave height from lowering it by as much as 50 cm (mostly offshore), compared to the control run, to increasing it up to 100 cm (nearshore). The relative differences of up to 20% being distributed non-symmetrically. Considering the effect of surface currents only, the range was between −50 and 40 cm whereas the sea level induced changes were between −10 and 100 cm, compared to the control run. The differences in significant wave heights were favoured under a specific phase of inertial oscillation of the surface currents.

As the wave growth effect is concentrated in the narrow coastal zone, even a 0.5 nautical mile model grid was not accurate enough to capture all the local topographical features. For further studies of this kind, higher resolution models should be used and appropriate (directional) measurements in shallow water are needed for model validation.

Acknowledgment

We are grateful to Benjamin Matterson for providing language help.

References

Alari, V., 2013. Multi-scale wind wave modeling in the Baltic Sea. (PhD Dissertation). Tallinn Univ. Technol., 134 pp.

Baltic Sea Hydrographic Commission, 2013. Baltic Sea Bathymetry Database version 0.9.3, (Downloaded from http://data.bshc.pro/ on 21.03.2015).

Battjes, J.A., Janssen, J.P.F.M., 1978. Energy loss and set-up due to breaking of random waves. In: Proc. of the 16th International Conference on Coastal Engineering. 569—587, http://dx.doi.org/10.1061/9780872621909.034.

Booij, N., Ris, R.C., Holthuijsen, L.H., 1999. A third-generation wave model for coastal regions: 1. Model description and validation. J. Geophys. Res. 104 (C4), 7649—7666, http://dx.doi.org/10.1029/98JC02622.

Bretherton, F.P., Garrett, C.J.R., 1968. Wavetrains in inhomogeneous moving media. Proc. Roy. Soc. A: Math. Phys. 302 (1471), 529—554, http://dx.doi.org/10.1098/rspa.1968.0034.

Feistel, R., Nausch, G., Wasmund, N., 2008. State and Evolution of the Baltic Sea, 1952—2005: A Detailed 50-year Survey of Meteorology and Climate, Physics, Chemistry, Biology and Marine Environment. John Wiley & Sons, Hoboken, 712 pp.

Feser, F., Barcikowska, M., Krueger, O., Schenk, F., Weisse, R., Xia, L., 2015. Storminess over the North Atlantic and northwestern Europe — a review. Q. J. Roy. Meteor. Soc. 141 (687), 350—382, http://dx.doi.org/10.1002/qj.2364.

Funkquist, L., Kleine, E., 2007. An introduction to HIROMB, an operational baroclinic model for the Baltic Sea. SMHI Rep. Oceanogr. 37, 1—39.

Guedes Soares, C., de Pablo, H., 2006. Experimental study of the transformation of wave spectra by a uniform current. Ocean Eng. 33 (3—4), 293—310, http://dx.doi.org/10.1016/j.oceaneng.2005.05.005.

Hasselmann, K., 1974. On the spectral dissipation of ocean waves due to whitecapping. Bound.-Lay. Meteorol. 6 (1), 107—127, http://dx.doi.org/10.1007/BF00232479.

Hasselmann, K., Barnett, T.P., Bouws, E., Carlson, H., Cartwright, D. E., Enke, K., Ewing, J.A., Gienapp, H., Hasselmann, D.E., Kruseman, P., Meerburg, A., 1973. Measurements of Wind-Wave Growth and Swell Decay During the Joint North Sea Wave Project (JONSWAP). Deutches Hydrogr. Inst.

Jaagus, J., Kull, A., 2011. Changes in surface wind directions in Estonia during 1966—2008 and their relationships with large-scale atmospheric circulation. Est. J. Earth Sci. 60 (4), 220—231, http://dx.doi.org/10.3176/earth.2011.4.03.

Kahma, K.K., Petterson, H., 1993. Wave Statistics from the Gulf of Finland. Finnish Inst. Marine Rep., Intern. Rep. 1.

Lagemaa, P., 2012. Operational forecasting in Estonian marine waters. (Ph.D. diss.). Tallinn Univ. Tech., 130 pp.

Leppäranta, M., Myrberg, K., 2009. Physical Oceanography of the Baltic Sea. Springer-Verlag, Berlin, Heidelberg, 378 pp., http://dx.doi.org/10.1007/978-3-540-79703-6.

Longuet-Higgins, M.S., Stewart, R.W., 1960. Changes in the form of short gravity waves on long waves and tidal currents. J. Fluid Mech. 8 (4), 565—583, http://dx.doi.org/10.1017/S0022112060000803.

Longuet-Higgins, M.S., Stewart, R.W., 1961. The changes in amplitude of short gravity waves on steady non-uniform currents. J. Fluid Mech. 10 (4), 529—549, http://dx.doi.org/10.1017/S0022112061000342.

Longuet-Higgins, M.S., Stewart, R.W., 1964. Radiation stresses in water waves; a physical discussion, with applications. Deep Sea Res. Oceanogr. Abstr. 11 (4), 529—562, http://dx.doi.org/10.1016/0011-7471(64)90001-4.

Miles, J.W., 1957. On the generation of surface waves by shear flows. J. Fluid Mech. 3 (2), 185—204, http://dx.doi.org/10.1017/S0022112057000567.

Phillips, O.M., 1957. On the generation of waves by turbulent wind. J. Fluid Mech. 2 (5), 417—445, http://dx.doi.org/10.1017/S0022112057000233.

Raudsepp, U., Laanemets, J., Haran, G., Alari, V., Pavelson, J., Kõuts, T., 2011. Flow, waves, and water exchange in the Suur Strait, Gulf of Riga, in 2008. Oceanologia 53 (1), 35—56, http://dx.doi.org/10.5697/oc.53-1.035.

Soomere, T., Behrens, A., Tuomi, L., Nielsen, J.W., 2008. Wave conditions in the Baltic Proper and in the Gulf of Finland during windstorm Gudrun. Nat. Hazards Earth Syst. 8 (1), 37—46, http://dx.doi.org/10.1016/j.ecss.2014.08.001.

Suursaar, Ü., 2013. Locally calibrated wave hindcasts in the Estonian coastal sea in 1966—2011. Est. J. Earth Sci. 62 (1), 42—56, http://dx.doi.org/10.5697/oc.54-3.421.

Suursaar, Ü., Kullas, T., Aps, R., 2012. Currents and waves in the northern Gulf of Riga: measurements and long-term hindcast. Oceanologia 54 (3), 421—447, http://dx.doi.org/10.5697/oc.54-3.421.

The SWAN team, 2013a. SWAN: Scientific and Technical Documentation. Cycle III version 40.91. Delft University of Technology, Department of Civil Engineering, The Netherlands.

The SWAN team, 2013b. SWAN: User Manual. Cycle III version 40.91. Delft University of Technology, Department of Civil Engineering, The Netherlands.

Tuomi, L., Pettersson, H., Fortelius, C., Tikka, K., Björkqvist, J.V., Kahma, K.K., 2014. Wave modelling in archipelagos. Coast. Eng. 83, 205—220, http://dx.doi.org/10.1016/j.coastaleng.2013.10.011.

Unden, P., Rontu, L., Jarvinen, H., Lynch, P., Calvo, J., Cats, G., Cuxart, J., Eerola, K., Fortelius, C., Garcia-Moya, J.A., Jones, C., Lenderlink, G., McDonald, A., McGrath, R., Navascues, B., Nielsen, N.W., Odegaard, V., Rodriguez, E., Rummukainen, M.A., 2002. HIRLAM-5 Scientific Documentation. Swedish Meteorol. Hydrol. Inst., Sweden.

Van der Westhuysen, A.J., 2012. Spectral modeling of wave dissipation on negative current gradients. Coast. Eng. 68, 17—30, http://dx.doi.org/10.1016/j.coastaleng.2012.05.001.

Whitham, G.B., 1974. Linear and Nonlinear Waves. John Wiley, New York, 55 pp.

Wolf, J., Prandle, D., 1999. Some observations of wave—current interaction. Coast. Eng. 37 (3), 471—485, http://dx.doi.org/10.1016/S0378-3839(99)00039-3.

Wolski, T., Wiśniewski, B., Giza, A., Kowalewska-Kalkowska, H., Boman, H., Grabbi-Kaiv, S., Hammarklint, T., Holfort, J., Lydeikaite, Ž., 2014. Extreme sea levels at selected stations on the Baltic Sea coast. Oceanologia 56 (2), 259—290, http://dx.doi.org/10.5697/oc.56-2.259.